The Astrophysical Journal, 718:467–473, 2010 July 20 doi:10.1088/0004-637X/718/1/467

MULTIBAND NONTHERMAL RADIATIVE PROPERTIES OF HESS J1813-178

Jun Fang and Li Zhang
Department of Physics, Yunnan University, Kunming, China; lizhang@ynu.edu.cn
Received 2009 November 6; accepted 2010 May 16; published 2010 July 1

ABSTRACT

The source HESS J1813-178 was detected in a survey of the inner Galaxy in TeV γ-rays, and a composite supernova remnant (SNR) G12.8-0.0 was identified in the radio band to be associated with it. The pulsar wind nebula (PWN) embedded in the SNR is powered by an energetic pulsar PSR J1813-1749, which was recently discovered. Whether the TeV γ-rays originate from the SNR shell or the PWN is currently uncertain. We theoretically investigate the multiwavelength nonthermal radiation from the composite SNR G12.8-0.0. The emission from the particles accelerated in the SNR shell is calculated by applying a semianalytical method to the nonlinear diffusive shock acceleration mechanism. In the model, the magnetic field is self-generated via resonant streaming instability, and the dynamical reaction of the field on the shock is taken into account. Based on a model which couples the dynamical and radiative evolution of a PWN in a non-radiative SNR, the dynamics and the multiband emission of the PWN are investigated. The particles are injected with the spectrum of a relativistic Maxwellian plus a power-law high-energy tail with an index of -2.5. Our results indicate that the radio emission from the shell can be reproduced well as synchrotron radiation of the electrons accelerated by the SNR shock; with an interstellar medium number density of 1.4 cm^{-3} for the remnant, the γ-ray emission from the SNR shell is insignificant and the observed X-rays and very high energy (VHE) γ-rays from the source are consistent with the emission produced by electrons/positrons injected in the PWN via synchrotron radiation and inverse Compton scattering, respectively; the resulting γ-ray flux for the shell is comparable to the detected one, only with a relatively larger density of about 2.8 cm^{-3}. The VHE γ-rays of HESS J1813-178 can be naturally explained to mainly originate from the nebula, although the contribution of the SNR shell becomes significant with a denser ambient medium.

Key words: gamma rays: ISM – ISM: individual objects (HESS J1813-178, G12.8-0.0) – ISM: supernova remnants

Online-only material: color figures

1. INTRODUCTION

The very high energy (VHE) source HESS J1813-178 was discovered with the High Energy Stereoscopic System (H.E.S.S.) in a survey of the inner Galaxy in VHE γ-rays (Aharonian et al. 2005a). The VHE γ-ray image obtained with H.E.S.S. shows a pointlike source with an extension of $\sim 2\farcm2$ and the observed spectrum has a hard photon index of 2.09 ± 0.08 (Aharonian et al. 2006). HESS J1813-178 was also detected in VHE γ-rays with the Major Atmospheric Gamma Imaging Cerenkov (MAGIC) telescope. The differential flux given by MAGIC between 0.4 and 10 TeV can be described well by a power law with an index of -2.1 ± 0.2 (Albert et al. 2006), which is consistent with the result obtained with H.E.S.S..

At first, HESS J1813-178 was unidentified and it was assumed to be a "dark particle accelerator" since no counterpart at lower frequencies was ever reported. However, the shell of SNR G12.8-0.0 associated with HESS J1813-178 was discovered with a diameter of $\sim 2\farcm5$ in a new low-frequency Very Large Array (VLA) 90 cm survey (Brogan et al. 2005). The nonthermal radio flux densities of the shell-type SNR are 0.65 ± 0.10 and 1.2 ± 0.08 Jy at 20 and 90 cm, respectively (Brogan et al. 2005). A highly absorbed X-ray source AX J1813-178, for which the column density is 10^{23} cm^{-2}, detected with *ASCA* is spatially coincident with the supernova remnant (SNR). The X-ray emission extending to 10 keV with a sharp cutoff below 2 keV is primarily nonthermal, meaning it can originate either from the SNR shell or from the pulsar wind nebula (PWN) inside the remnant (Brogan et al. 2005). Due to the high column density derived from the *ASCA* data, a distance of $\geqslant 4$ kpc is derived for the source (Brogan et al. 2005).

Moreover, a soft γ-ray source, IGR J18135-1751, was discovered as the counterpart of HESS J1813-178 (Ubertini et al. 2005). It is persistent with a 20–100 keV luminosity of 5×10^{34} erg s^{-1} for a distance of 4 kpc. Ubertini et al. (2005) argued that the observed properties of the source in the radio and X-ray bands can be explained with the assumption that the source is a PWN embedded in G12.8-0.0. Furthermore, high angular resolution X-ray observation with *XMM-Newton* shows that the X-ray emitting object appears as a compact core located in the center of the radio shell-type SNR G12.8-0.0 (Funk et al. 2007). They argued that the source is a composite SNR since the central object shows morphological and spectral resemblance to a PWN.

The *Chandra* observation of SNR G12.8-0.0 indicates that the X-ray source is a point surrounded by structured diffuse emission that fills the interior of the radio shell (Helfand et al. 2007). The compact source has a spectrum characterized by a power law with an index of ~ 1.3, typical of young and energetic rotation-powered pulsars, and the morphology of the diffuse emission strongly resembles that of a PWN (Helfand et al. 2007). Recently, an energetic pulsar PSR J1813-1749 with a period of ~ 44.7 ms, a characteristic age of 3.3–7.5 kyr, and a distance of 4.7 kpc estimated by assuming an association with an adjacent young stellar cluster, was discovered in a long, continuous *XMM-Newton* X-ray timing observation (Gotthelf & Halpern 2009). The pulsar was found to be associated with SNR G12.8-0.0 and it powers the PWN (Gotthelf & Halpern 2009).

High-energy γ-rays can be produced either from SNR shells in which particles are accelerated to relativistic speeds through the first *Fermi* process (e.g., Aharonian et al. 2005b, 2007; Berezhko & Völk 2006; Fang & Zhang 2008; Fang et al.

2009; Morlino et al. 2009a) or from PWNe powered by the pulsars inside them (e.g., Volpi et al. 2008; Zhang et al. 2008; Gelfand et al. 2009). Although the source HESS J1813-178 is pointlike in VHE γ-rays, the possibility of the VHE γ-rays originating from the shell of the remnant cannot be ruled out given the size of the SNR, the angular resolution of the H.E.S.S. telescope, and the depth of the observations (Albert et al. 2006). In this paper, we study the multiband nonthermal emission from the shell of SNR G12.8-0.0 and the nebula inside it. The emission from the particles accelerated by the SNR shock is investigated by applying a semianalytical method to the nonlinear diffusive shock acceleration mechanism with a free escape boundary proposed by Caprioli et al. (2010b), in which the amplified magnetic field due to resonant streaming instability induced by cosmic rays and the dynamical feedback of this self-generated magnetic field on the shock are taken into account. On the other hand, the dynamics and the multiband radiative properties of the PWN are basically investigated according to the model in Gelfand et al. (2009), which can self-consistently describe the dynamical and radiative evolution of a PWN in a non-radiative SNR. Recently, based on the long-term two-dimensional particle-in-cell simulations, Spitkovsky (2008) found that the particle spectrum downstream of a relativistic shock consists of two components: a relativistic Maxwellian and a power-law high-energy tail with an index of -2.4 ± 0.1. In contrast to Gelfand et al. (2009), in which a single power-law injection spectrum for the electrons/positrons is employed to discuss the radiative properties during different phases of the PWN, in this paper we argue that the high-energy particles are injected with the spectrum of a relativistic Maxwellian plus a power-law high-energy tail during the evolution, and a kinetic equation is used to obtain the energy distribution of the particles.

2. MODEL AND RESULTS

In this section, we describe the physics of our model for the particles accelerated by a shock and its multiband nonthermal emission (Section 2.1), the dynamics and multiwavelength radiation of a PWN in the nonradiative shell (Section 2.2), and its implementation to SNR G12.8-0.0 (Section 2.3).

2.1. Particles Accelerated by the SNR Shock and its Emission

The pitch-angle averaged steady-state distribution of the protons accelerated at a shock in one dimension satisfies the diffusive transport equation (Malkov & Drury 2001; Blasi 2002; Amato et al. 2008)

$$\frac{\partial}{\partial x}\left[D\frac{\partial}{\partial x}f(x,p)\right] - u\frac{\partial f(x,p)}{\partial x} + \frac{1}{3}\frac{du}{dx}p\frac{\partial f(x,p)}{\partial p} + Q(x,p) = 0, \quad (1)$$

where the coordinate x is directed along the shock normal from the downstream toward the upstream, D is the diffusion coefficient, and u is the fluid velocity in the shock frame, which equals u_2 downstream ($x > 0$) and changes continuously upstream from u_1 immediately upstream ($x = 0^-$) of the subshock to u_0 at far upstream. For the Bohm diffusion, $D = pc^2/(3eB)$, where B is the local magnetic field strength. The maximum momentum of protons accelerated by an SNR increases with time in the free-expansion phase of the SNR due to the efficient magnetic field strength and the constant shock speed. After the beginning of the Sedov–Taylor phase, the maximum momentum drops with time due to the decrease of the shock speed and the efficiency of the magnetic field amplification (Caprioli et al. 2009, 2010a). In this case, particles with higher momentum will escape from the SNR and this phenomenon can be mimicked by imposing a free escape boundary at a location upstream of the shock, i.e., $f(-x_0, p) = 0$ (Caprioli et al. 2010a, 2010b).

With the assumption that the particles are injected immediately upstream of the subshock, the source function can be written as $Q(x, p) = Q_0(p)\delta(x)$. For monoenergetic injection, $Q_0(p)$ is

$$Q_0(p) = \frac{\eta n_{\rm gas,1} u_1}{4\pi p_{\rm inj}^2}\delta(p - p_{\rm inj}), \quad (2)$$

where $p_{\rm inj}$ is the injection momentum, $n_{\rm gas,1}$ is the gas density at $x = 0^+$, and η is the fraction of particles injected in the acceleration process. With the injection recipe known as thermal leakage, η can be described as $\eta = 4(R_{\rm sub} - 1)\xi^3 e^{-\xi^2}/3\pi^{1/2}$ (Blasi et al. 2005; Amato et al. 2008), where $R_{\rm sub} = u_1/u_2$ is the compression factor at the subshock and ξ is a parameter on the order of 2–4 describing the injection momentum of the thermal particles in the downstream region ($p_{\rm inj} = \xi p_{\rm th,2}$). $p_{\rm th,2} = (2m_p k_{\rm B} T_2)^{1/2}$ is the thermal peak momentum of the particles in the downstream fluid with temperature T_2, m_p is the proton mass, and $k_{\rm B}$ is the Boltzmann constant. The downstream temperature, T_2, is calculated with Equations (10) and (11) in Caprioli et al. (2009). A relatively large $\xi = 3.8$–4.1 is usually employed to investigate the radiative properties of SNRs (e.g., Morlino et al. 2009a, 2009b) and we adopt $\xi = 3.8$ in this paper.

The normalized pressure in cosmic rays is

$$P_c(x) = \frac{4\pi}{3\rho_0 u_0^2}\int_{p_{\rm inj}}^{\infty} dp p^3 v(p) f(x,p), \quad (3)$$

where ρ_0 is the gas density far upstream of the shock. Magnetic fields can be generated by streaming instability induced by the accelerated particles. With the assumption that the turbulence is generated by the resonant streaming instability, the normalized pressure of the amplified magnetic field can be described as (Caprioli et al. 2009, 2010b)

$$P_w(x) = \frac{v_A}{4u_0}\frac{1 - U^2(x)}{U^{3/2}(x)}, \quad (4)$$

where $U(x) = u(x)/u_0$, $v_A = B_0/(4\pi\rho_0)^{1/2}$ is the Alfvén velocity, and B_0 is the background magnetic field strength. Then the strength of the amplified field is $\delta B(x) = (8\pi\rho_0 u_0^2 P_w(x))^{1/2}$ and the magnetic field downstream of the shock is further enhanced by $B_2 = R_{\rm sub} B_1$ (Morlino et al. 2009a), where $B_1 = \delta B(0)$ is the amplified magnetic field immediately upstream of the subshock. The effect of turbulent heating is ignored in this paper because the properties of the damping of the magnetic field are still uncertain, and a new parameter is needed even with the damping phenomenologically taken into account (Caprioli et al. 2010a). Neglecting the effect of turbulent heating, the normalized pressure of the background gas is

$$P_g(x) = \frac{U(x)^{-\gamma}}{\gamma M_0^2}, \quad (5)$$

where M_0 is the sonic Mach number of the shock and $\gamma = 5/3$ is the adiabatic index. The total compression factor $R_{\rm tot}$ is

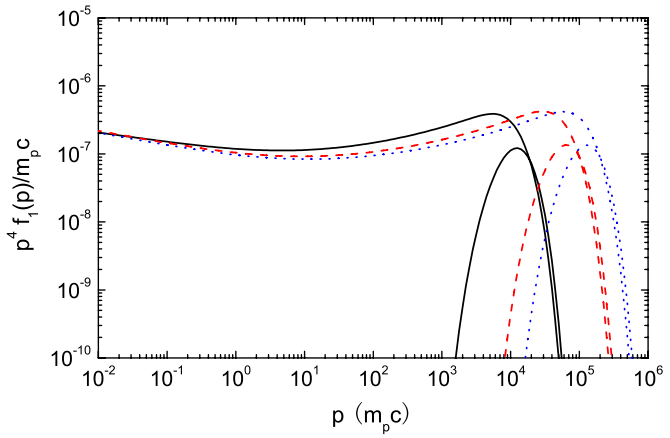

Figure 1. Particle spectra at the shock and the escape fluxes ($p^4\phi_{\rm esc}/u_0$) with $\xi = 3.8$, $T_0 = 10^4$ K, $n_0 = 1.4$ cm^{-3}, $B_0 = 5\,\mu$G, $u_0 = 1 \times 10^8$ cm s^{-1}, $x_0 = 0.18$ pc (solid line); $x_0 = 0.9$ pc (dashed line); and $x_0 = 1.8$ pc (dotted line).

(A color version of this figure is available in the online journal.)

related with the compression factor at the subshock $R_{\rm sub}$ through (Caprioli et al. 2009)

$$R_{\rm tot}^{\gamma+1} = \frac{M_0^2 R_{\rm sub}^{\gamma}}{2}\left[\frac{\gamma + 1 - R_{\rm sub}(\gamma-1)}{1+\Lambda_B}\right], \quad (6)$$

where

$$\Lambda_B = \frac{P_w(0)}{P_g(0)}[1 + R_{\rm sub}(2/\gamma - 1)]. \quad (7)$$

Given a value of ξ, a temperature far upstream of the shock T_0, a shock velocity u_0, a background magnetic field B_0, and x_0, the particle spectrum at the shock $f_1(p)$ and the escape flux $\phi_{\rm esc}(p) = -[D(x, p)\partial f/\partial x]_{x_0}$ can be obtained with the method proposed in Caprioli et al. (2010b), in which the diffusion coefficient is calculated in the self-generated magnetic field induced by resonant streaming instability of the accelerated particles. In order to show how the proton spectrum is affected by the choice of x_0, we plot in Figure 1 the particle spectra at the subshock position and the escaping fluxes for three different values of x_0: 0.18 pc (solid line); 0.9 pc (dashed line); and 1.8 pc (dotted line). The other parameters are all fixed to: $\xi = 3.8$, $T_0 = 10^4$ K, $n_0 = 1.4$ cm^{-3}, $B_0 = 5\,\mu$G, $u_0 = 1 \times 10^8$ cm s^{-1}. The particle spectrum for each x_0 is cut off at a maximum momentum $p_{\rm max}$, which increases with the value of x_0. $U(x)$, $P_c(x)$, and δB in the upstream region for $x_0 = 0.9$ pc are indicated in Figure 2. The amplified magnetic field immediately upstream of the subshock B_1 is 56 μG, which is significantly stronger than the background magnetic field.

The electrons have the same spectrum of the protons up to a maximum energy determined by synchrotron losses. Note that the spectrum of the accelerated electrons at the shock around the cutoff momentum $p_{{\rm max},e}$ is difficult to obtain in a fully nonlinear scenario. With the test particle approximation, the energy spectrum of electrons accelerated by SNR shocks for a strong shock can be described as (Zirakashvili & Aharonian 2007; Blasi 2010)

$$f_e(x, p) = K_{ep} f(x, p)[1 + 0.523(p/p_{{\rm max},e})^2] \times \exp\left(-p^2/p_{{\rm max},e}^2\right). \quad (8)$$

However, the spectrum cut off by a simple exponential is also employed to reproduce the multiband emission from SNRs (e.g.,

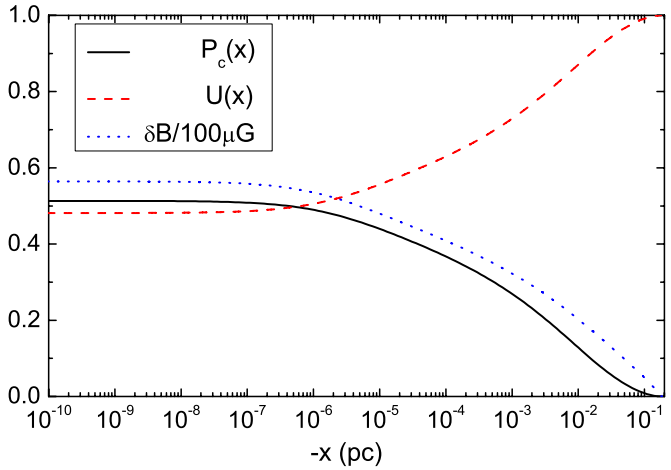

Figure 2. $P_c(x)$ (solid line), $U(x)$ (dashed line), and $\delta B/100\,\mu$G (dotted line) in the upstream region for $x_0 = 0.9$ pc. The others are the same as Figure 1.

(A color version of this figure is available in the online journal.)

Fang et al. 2009) and we use this form in this paper, i.e.,

$$f_e(x, p) = K_{ep} f(x, p) \exp(-E(p)/E_{{\rm max},e}), \quad (9)$$

where $E(p)$ is the kinetic energy of the electrons and the electron/proton ratio K_{ep} is treated as a parameter. The choice of the cutoff shape of the spectrum has no influence on our results because in this paper we interpret the observed X-ray from emission G12.8-0.0 as due to the PWN inside the remnant. The maximum energy of electrons results in equating the synchrotron loss time with the acceleration time. In the context of nonlinear shock acceleration an approximate solution is given by the following equation (Berezhko et al. 2002)

$$E_{{\rm max},e} = 6 \times 10^7 \left(\frac{u_0}{10^8\ {\rm cm\ s^{-1}}}\right) \times \left[\frac{R_{\rm tot} - 1}{R_{\rm tot}(1 + R_{\rm sub} R_{\rm tot})}\left(\frac{10\,\mu{\rm G}}{B_1}\right)\right]^{1/2} {\rm MeV}, \quad (10)$$

where the magnetic field immediately upstream of the shock, B_1, is assumed to be compressed by a factor $R_{\rm sub}$.

Assuming that the accelerated particles distribute homogeneously and most of the emission is from downstream of the shock, and using the distribution function at the shock to represent the particle distribution in the whole emitting zone, the volume-averaged emissivity for photons produced via p–p interactions can be written as

$$Q(E) = 4\pi n_{\rm gas} \int dE_p J_p(E_p) \frac{d\sigma(E, E_p)}{dE}, \quad (11)$$

where E_p is the proton kinetic energy, $n_{\rm gas} = R_{\rm tot} n_0$ is the gas number density downstream of the shock, and $J_p(E_p) = vp^2 f_0(p) dp/dE_p$ is the volume-averaged proton density where v is the particles' velocity. We use the differential cross section for photons $d\sigma(E, E_p)/dE$ presented in Kamae et al. (2006) to calculate the hadronic γ-rays produced via p–p interaction. Finally, the photon flux observed at the Earth can be obtained with

$$F(E) = \frac{V Q(E)}{4\pi d^2}, \quad (12)$$

where d is the distance from the earth to the source and V is the average emitting volume of the source. For the accelerated protons, the emitting volume can be estimated by $V_p \approx$

$(4\pi/3)R_{\rm snr}^3/R_{\rm tot}$ (Ellison et al. 2000), where $R_{\rm snr}$ is the radius of the SNR. For the electrons, the thickness of the emitting region can be estimated by solving the diffusion-convection equation downstream of the shock, i.e., $u_2(\partial f_e/\partial x) = D\partial^2/\partial x^2 - f_e/\tau_{\rm syn}$, where $\tau_{\rm syn}$ is the time scale of the synchrotron radiation (Morlino et al. 2009a). The solution shows $f_e \propto \exp(-x/R_{\rm rim})$ and the spatial scale $R_{\rm rim}$ is given by (Berezhko & Völk 2004)

$$R_{\rm rim}(p) = \frac{2D_2/u_2}{\sqrt{1+4D_2/u_2\tau_{\rm syn}}-1}. \quad (13)$$

As a result of the synchrotron losses, electrons with relatively high energy are confined to a thin rim behind the shock and the total emitting volume is smaller than V_p. A break in the spectrum occurs for $p = p_t$, defined as the momentum where the time scale of the losses equals the age of the remnant, i.e., $\tau_{\rm syn}(p_t) = t_{\rm snr}$. In the steady state, the volume of the electrons with higher energies is smaller than that of the protons due to the strong synchrotron losses. Hence, $V_e(p) = V_p$ for $p \leqslant p_t$, while $V_e(p) = V_p R_{\rm rim}(p)/(R_{\rm snr}/3R_{\rm tot})$ for $p > p_t$, where p_t is determined by $4\pi R_{\rm snr}^2 R_{\rm rim}(p) = V_p$.

2.2. Dynamics and Radiative Properties of a PWN Inside a Nonradiative SNR

A PWN is powered by a pulsar that dissipates its rotational energy into the nebula. The spin-down luminosity of a pulsar with a rotation period P evolves with time as (e.g., Gaensler & Slane 2006; Slane 2008)

$$\dot{E}(t) = \dot{E}_0\left(1+\frac{t}{\tau_0}\right)^{-\frac{n+1}{n-1}}, \quad (14)$$

where τ_0 is the spin-down time scale of the star, $\dot{E}_0$ is the initial spin-down power, and n is the braking index of the pulsar, which is equal to 3 for magnetic dipole spin-down.

High-energy particles and magnetic fluxes are injected into the PWN from the termination shock (TS) located where the ram pressure of the unshocked wind is equal to that of the nebula. In this paper, we assume that the spin-down power is distributed between electrons and positrons ($\dot{E}_{\rm e}(t) = \eta_{\rm e}\dot{E}(t)$) and magnetic fields ($\dot{E}_{\rm b} = \eta_{\rm b}\dot{E}(t)$; e.g., Gelfand et al. 2009). In Gelfand et al. (2009), they used a simple power-law injection spectrum for the electrons/positrons to discuss the radiative properties during different phases of the PWN. However, a broken power-law spectrum is usually needed to reproduce the nonthermal emission of a PWN with multiband observations (e.g., Atoyan & Aharonian 1996; Venter & de Jager 2006; Slane et al. 2008; Zhang et al. 2008). Recently, based on the long-term two-dimensional particle-in-cell simulations, Spitkovsky (2008) found that the particle spectrum downstream of a relativistic shock is a Maxwellian plus a power-law tail with an index of 2.4 ± 0.1, and this spectrum was also used to investigate the multiband emission from PWNe (e.g., Fang & Zhang 2010; Slane et al. 2010). We assume that high-energy particles injected in a PWN are accelerated by the TS, which is typically relativistic with a lorentz factor $\sim 10^6$ with respect to the pulsar wind upstream of the shock. Therefore, we assume that the spectrum of the high-energy particles injected in the PWN has the form

$$Q(E,t) = \begin{cases} C(t)\frac{E}{E_{\rm b}}\exp\left(-\frac{E}{E_{\rm b}}\right) & E \leqslant E_{\rm min} \\ C(t)\left[\frac{E}{E_{\rm b}}\exp\left(-\frac{E}{E_{\rm b}}\right) + f\left(\frac{E}{E_{\rm b}}\right)^{-\alpha}\right] & E_{\rm min} < E \leqslant E_{\rm max} \end{cases}, \quad (15)$$

Table 1
Input Parameters for the SNR G12.8-0.0

Parameter	Value	Parameter	Value
d	4.7 kpc	$\dot{E}_0$	4.2×10^{38} erg s^{-1}
$E_{\rm sn}$	0.4×10^{50}erg	$\tau_{\rm sd}$	500 yr
$M_{\rm ej}$	3 $M_\odot$	n	3.0
n_0	1.4 cm^{-3}	$\eta_{\rm B}$	1×10^{-4}
Age	1200 yr	$E_{\rm max}$	1000 TeV
T_0	10^4 K	$E_{\rm b}$	3×10^5 MeV
B_0	5 μG	$v_{\rm psr}$	120 km s^{-1}
K_{ep}	1.8×10^{-3}		

where $\alpha = 2.4 \pm 0.1$, $E_{\rm b} \sim 2.6 \times 10^5 \gamma_{\rm ts,6}$ MeV, $\gamma_{\rm ts,6}$ is the Lorentz factor of the upstream pulsar wind of the TS in units of 10^6, $E_{\rm min} = f_{\rm min}E_{\rm b}$ with $f_{\rm min} \sim 7$, f is normalized by $E_{\rm min}/E_{\rm b}\exp(-E_{\rm min}/E_{\rm b}) = f(E_{\rm min}E_{\rm b})^{-\alpha}$. $C(t)$ can be obtained with

$$C(t) = \frac{\dot{E}_{\rm e}(t)}{2E_{\rm b}^2 + f\frac{E_{\rm b}^2}{2-\alpha}\left[\left(\frac{E_{\rm max}}{E_{\rm b}}\right)^{2-\alpha} - \left(\frac{E_{\rm min}}{E_{\rm b}}\right)^{2-\alpha}\right]}. \quad (16)$$

Assuming that the particles injected in the nebula are homogeneously distributed, the energy distribution of these particles in the nebula evolves as

$$\frac{\partial N(E,t)}{\partial t} = \frac{\partial}{\partial E}[\dot{E}N(E,t)] + Q(E,t), \quad (17)$$

where $\dot{E}$ is the energy-loss rate of the particles with energy E. Energy-loss mechanisms include synchrotron radiation, IC scattering, and adiabatic loss.

The dynamics of the PWN inside the supernova shell is basically calculated following the model presented in Gelfand et al. (2009). The model assumes that the progenitor supernova ejects material with mass $M_{\rm ej}$ and energy $E_{\rm sn}$ into the ambient matter with a constant density $\rho_{\rm ISM}$. Assuming the PWN has no influence on the dynamics of the forward shock and the reverse shock, the velocity and the radius of the forward shock and the reverse shock of the surrounding SNR are calculated with the equations in Truelove & McKee (1999). The pulsar dissipates energy into the PWN, which sweeps up the supernova ejecta into a thin shell surrounding the nebula, and new particles are injected into the PWN at each time step.

The dynamical evolution of the PWN with the parameters for SNR G12.8-0.0 (see Table 1) is shown in Figure 3. The radii of the SNR ($R_{\rm snr}$), the reverse shock ($R_{\rm rs}$), the PWN ($R_{\rm pwn}$), and the pulsar are indicated by the dashed, dotted, solid and dash-dotted lines, respectively. A velocity of 120 km s^{-1} is used in the calculation, which has no influence on the resulting dynamical structure and radiative property of G12.8–0.0 because the young pulsar is safely in the nebula now (see Section 2.3). Initially, the pressure of the PWN is much greater than the pressure of the surrounding supernova ejecta, so the PWN expands adiabatically into the cold supernova ejecta. The ejecta surrounding the PWN is swept up to a thin shell, which is decelerated by ram pressure since its velocity is higher than the local sound speed (Gelfand et al. 2007). The mass of the PWN $M_{\rm pwn}$ increases continuously since the shell expands faster than the ambient ejecta. This expansion phase ends when the PWN collides with the reverse shock of the SNR. After the collision, the pressure inside the nebula, $P_{\rm pwn}$, is much smaller than the pressure of the material around it, $P_{\rm snr}(R_{\rm pwn})$. The velocity of the PWN decreases greatly, and finally the PWN is compressed.

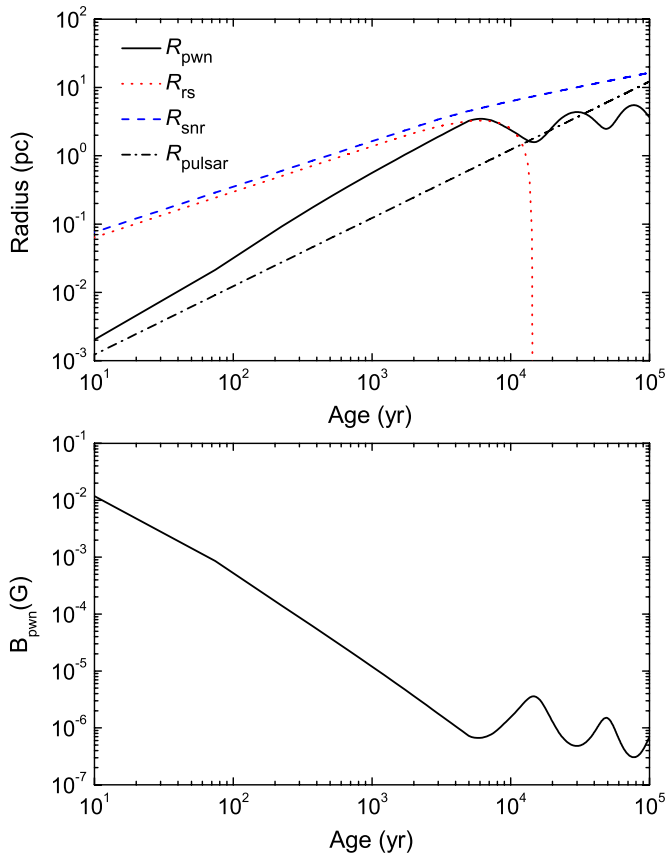

Figure 3. Upper panel: radius of the SNR (R_{snr}; dashed line), reverse shock (R_{rs}; dotted line), PWN (R_{pwn}; solid line), and the location of the pulsar (R_{pulsar}; dash-dotted line). Lower panel: magnetic field strength in the PWN (B_{pwn}).
(A color version of this figure is available in the online journal.)

During this process of compression, the magnetic field strength in the nebula increases significantly. Furthermore, the radius of the PWN decreases significantly, and the PWN will expand again when the inner pressure eventually becomes more than that of the surrounding ejecta. The nebula experiences a series of contractions and re-expansions until the SNR enters the radiative phase of its evolution. The pulsar moving in space will leave the PWN during the compression, and it can re-enter the nebula when the nebula expands again. With the parameters in Table 1, the pulsar first leaves the nebula at ∼13700 yr and re-enters it at ∼19000 yr.

2.3. Application to G12.8-0.0 and Discussion

The shell with a diameter of ∼2′.5, corresponding to a radius of 1.7 pc for a distance of 4.7 kpc of SNR G12.8-0.0 had been revealed with the radio observations with a spectral index of ∼−0.48 (Brogan et al. 2005). Moreover, a PWN with a diameter of ∼80″ embedded in the SNR was disclosed in the observations from the X-ray to soft γ-ray bands (Ubertini et al. 2005; Funk et al. 2007; Helfand et al. 2007). An energetic pulsar with a spin-down power greater than 10^{37} erg s^{-1} is argued to exist in the nebula based on the *ASCA* and *Chandra* observations (Helfand et al. 2007). Recently, the energetic pulsar PSR J1813-1749 associated with the PWN was discovered in the long, continuous *XMM-Newton* X-ray timing observation, and the pulsar has a period of ∼44.7 ms, a spin-down age of 3.3–7.5 kyr, and a spin power of $(6.8 \pm 2.7) \times 10^{37}$ erg s^{-1} (Gotthelf & Halpern 2009).

The small radius places SNR G12.8-0.0 among the smallest known SNRs, which also suggests a young age for the remnant. In the model, the radius of the SNR is determined by the explosion energy, the mass of the ejecta, the ambient density, and the age of the system. We find that with $E_{sn} = 0.4 \times 10^{50}$ erg, $M_{ej} = 3\ M_{\odot}$, and an ambient ISM density $n_0 = 1.4$ cm^{-3}, the resulting radius of the SNR shell is ∼1.8 pc at an age of ∼1200 yr, which is consistent with the radius of the radio shell. With a larger explosion energy ($E_{sn} \geqslant 10^{50}$ erg) or a smaller ambient density ($n_0 \leqslant 0.1$ cm^{-3}), the age of the system, which is constrained by the radius of the SNR, is much smaller than the radius of the radio shell, and the resulting flux of X-ray emission from the PWN is usually much higher than the observed one by *XMM-Newton* (Funk et al. 2007) and *INTEGRAL* (Brogan et al. 2005) since the magnetic field is stronger for a smaller age (see the lower panel of Figure 3). A sub-energetic explosion with $E_{sn} \leqslant 10^{50}$ erg and a low ejecta mass $M_{ej} = 3\ M_{\odot}$ was also argued to exist from the multiwavelength study of the newly discovered SNR G310.0-1.6 (Renaud et al. 2010). With $\tau_{sd} = 500$ yr and $\dot{E}_0 = 4.2 \times 10^{38}$ erg s^{-1}, the spin-down power is 3.6×10^{37} erg s^{-1} at an age of 1200 yr from Equation (14), which is a little smaller than the present observed value, i.e., $(6.8 \pm 2.7) \times 10^{37}$ erg s^{-1} (Gotthelf & Halpern 2009). The radius of the PWN at this age is 0.7 pc and the ratio R_{pwn}/R_{snr} is ∼0.4. The resulting multiband radiation from the PWN in the composite SNR G12.8-0.0 at an age of 1200 yr is shown in the upper panel of Figure 4 with the parameters in Table 1. In the figure, we also plot the observed data from radio to TeV band for comparison. The data sources are reported in the figure caption. For each panel, the interstellar soft photons scattered in the IC process contain the cosmic microwave background (CMB), IR ($T_{IR} = 35$ K, $U_{IR} = 1.0$ eV cm^{-3}), and star light ($T_{st} = 3000$ K, $U_{st} = 1.5$ eV cm^{-3}). The observed emission detected with *XMM-Newton* and *INTEGRAL* from the X-ray to hard X-ray bands can be explained as the synchrotron radiation from the electrons injected in the PWN, although the resulting flux is a little higher than that observed with *XMM-Newton*. In the VHE γ-ray band, the photons are mainly produced via IC scattering of the electrons in the nebula on the CMB and IR photons from interstellar dust (Figure 5).

The upstream temperature for an SNR varies between ∼10^4 K for a typical ISM up to ∼10^7 K if the SNR expands in the hot bubble generated by the progenitor's wind (Chevalier & Liang 1989; Morlino et al. 2009a; Berezhko & Völk 2010). We assume that SNR G12.8-0.0 is expanding in the typical ISM with a temperature of ∼10^4 K to investigate the multiband nonthermal emission from the SNR shell. At an age of 1200 yr, the velocity of the SNR shock is ∼1000 km s^{-1}, corresponding to a Mach number of ∼86 for $T_0 = 10^4$ K. With these parameters, R_{tot} and R_{sub} are about 8.1 and 3.55, respectively, and the downstream temperature, T_2, is 3.8×10^6 K. Moreover, the maximum energies of the accelerated protons and electrons are about 60 TeV and 4 TeV, respectively. The energy contained in the protons accelerated by the shock is 5×10^{48} erg, and in the electrons is 6×10^{45} erg. Therefore, about 12% of the explosion energy E_{sn} has been converted to the kinetic energy of the particles. The amplified magnetic field strength immediately upstream of the subshock is 62 μG, and then the downstream magnetic field strength is 220 μG. With this downstream magnetic field strength and $K_{ep} = 1.8 \times 10^{-3}$, the flux points of the radio shell can be reproduced as synchrotron radiation of the electrons accelerated by the SNR forward shock wave; whereas the flux from p–p collisions of the accelerated protons on the

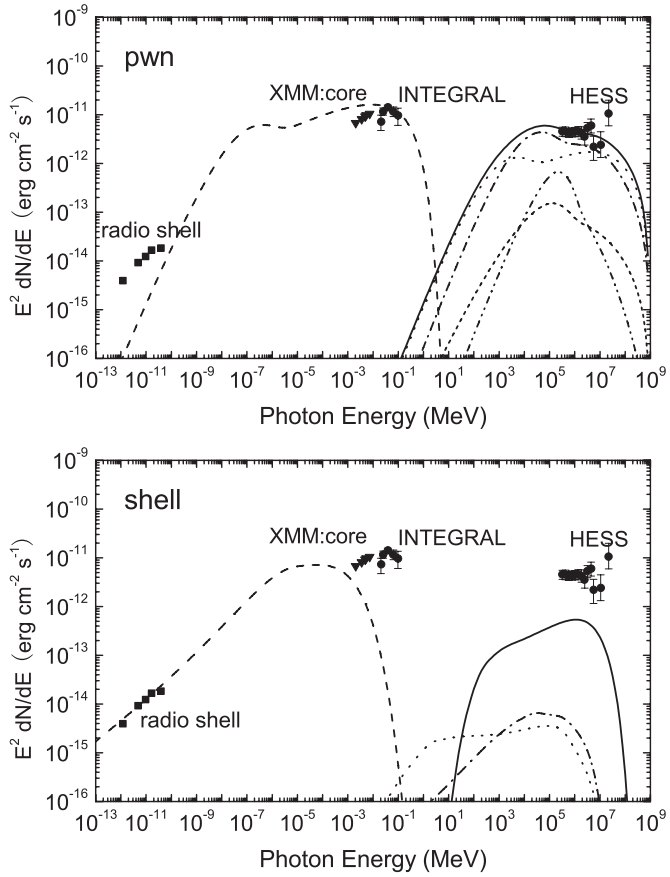

Figure 4. Upper panel: the spectral energy distribution for the PWN in G12.8-0.0 at an age of 1200 yr. Synchrotron radiation (dashed line), and IC scattering on the CMB (dotted line), IR (dash-dotted line), star light (dash-dot-dotted line), and the synchrotron photons (short dashed line) are shown in the figure. The solid line represents the whole IC scattering on all the soft photons. Lower panel: the spectral energy distribution of the emission from the shell of the SNR G12.8-0.0. Synchrotron radiation (dashed line), bremsstrahlung (dotted line), IC scattering (dash-dotted line) of the accelerated electrons, and *p*-*p* interactions (solid line) of the accelerated protons are demonstrated in the figure. The radio data are from the VLA, Bonn, Parkes, and Nobeyama observatories (Brogan et al. 2005). The X-ray data are from *XMM-Newton* (Funk et al. 2007) and *INTEGRAL* (Ubertini et al. 2005). The H.E.S.S. flux points in the VHE γ-ray band are from Aharonian et al. (2006).

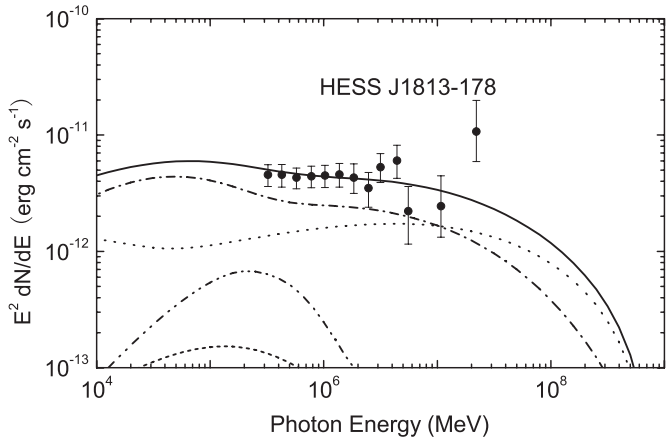

Figure 5. Zoomed view of the resulting spectrum and the H.E.S.S. results in the TeV band. The others are the same as the upper panel in Figure 4.

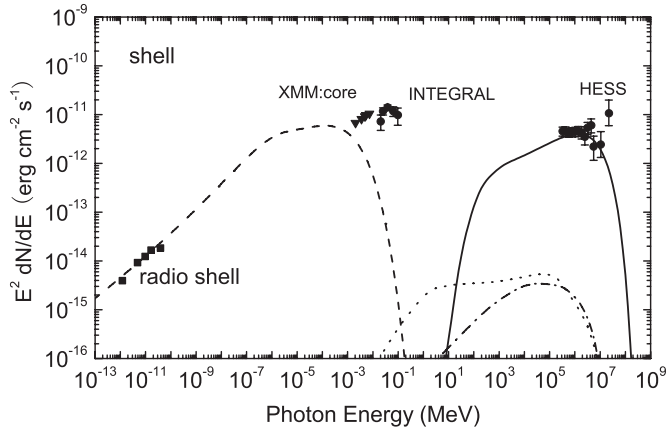

Figure 6. Spectral energy distribution of the emission from the shell for $n_0 = 2.8$ cm^{-3} and $K_{ep} = 4.5 \times 10^{-4}$. The others are the same as the lower panel of Figure 4.

ambient matter is significantly smaller than that observed with HESS.

The ISM number density n_0 is an important parameter that can greatly influence the multiband nonthermal emission from the SNR shell. With a larger n_0, both the density of the accelerated particles and the density of the matter downstream of the shock increase accordingly. As a result, the flux of the *p*–*p* collisions is enhanced with $\propto n_0^2$, and then a smaller K_{ep} is usually needed to reproduce the observed radio fluxes for a denser medium. In order to reproduce the H.E.S.S. flux in the TeV band via *p*–*p* collisions from protons accelerated by the SNR shell, a denser medium with a density of 2.8 cm^{-3} must be used in the model (see Figure 6). For $n_0 = 2.8$ cm^{-3} and the other parameters the same as Figure 4, the multiband nonthermal emission from the PWN is nearly the same as that for $n_0 = 1.4$ cm^{-3}, whereas the γ-ray flux for the *p*–*p* collisions in the SNR shell is comparable to the HESS result; the downstream magnetic field strength is 271 μG, and then a smaller $K_{ep} = 4.5 \times 10^{-4}$ is needed to reproduced the observed fluxes in the radio band. In this SNR-dominated scenario, the γ-ray photon index of the resulting emission is <2 up to several tens of GeV, whereas it is >2 at higher energies (Figure 6). On the other hand, the index in the PWN-dominated case is <2 from 0.1 GeV to 1 TeV (Figure 4). The resulting TeV γ-ray spectral energy distributions in the two scenarios are all consistent with the H.E.S.S. flux points, so we cannot determine which case is preferred by comparison with the detected fluxes in the TeV range now. However, the flux in the GeV band in the PWN-dominated case is several times higher than in the SNR-dominated case, so future detections in this band can put constraints on the origin of the γ-rays from HESS J1813-178.

Even if a denser medium with $n_0 \sim 2.8$ cm^{-3} is used in the model to enhance the *p*–*p* collisions in the SNR shell, the IC scattering of the electrons/positrons in the PWN is still prominent enough to contribute significantly to the high-energy γ-ray emission from the composite SNR. In the model, the PWN evolves in the remnant with an age of $\sim$1200 yr, and high-energy electrons/positrons are injected continuously into the nebula from the energetic pulsar during the evolution. In fact, if the emission detected with *XMM-Newton* and *INTEGRAL* is the synchrotron radiation from the electrons/positrons injected in the PWN, the detected VHE γ-rays can be easily explained by the IC scattering of these electrons/positrons off the ambient soft photons. Therefore, it is natural to argue that the observed high-energy photons from the X-ray to VHE γ-ray bands originate mainly from the PWN inside the composite remnant although the contribution of the SNR shell to the γ-rays becomes significant for a denser medium with a density of 2.8 cm^{-3}.

3. SUMMARY AND CONCLUSION

The origin of the VHE γ-rays from HESS J1813-178 is investigated in this paper. Although the source is pointlike in VHE γ-rays, a shell origin of the VHE γ-rays cannot be ruled out because the PSF of the H.E.S.S. telescope is very close to the size of the SNR's shell (e.g., Albert et al. 2006). An SNR with a diameter of 2.′5 was identified in the radio bands to be associated with the VHE γ-ray source. Moreover, X-ray observations showed that a PWN powered by an energetic pulsar is embedded in the SNR (Brogan et al. 2005; Ubertini et al. 2005; Funk et al. 2007; Helfand et al. 2007), and the pulsar was recently discovered in a long, continuous *XMM-Newton* X-ray timing observation (Gotthelf & Halpern 2009). We apply a model that can self-consistently calculate the multiwavelength nonthermal emission both from the SNR shell and from the PWN embedded in the remnant. In the model, electrons/positrons with the spectrum of a relativistic Maxwellian plus a power-law high-energy tail are injected in the nebula during the PWN during its evolution inside the SNR; protons and electrons are accelerated by the SNR shock wave, and the spectrum of the accelerated particles are calculated with a semianalytical nonlinear model. Our results indicate that with the parameters in Table 1, (1) the observed emission of the shell in the radio bands can be explained well as synchrotron radiation of the electrons accelerated by the SNR shock wave, whereas the flux of p–p collisions of the accelerated protons is significantly smaller than the TeV flux observed with H.E.S.S.; (2) the observed emission in the X-ray to hard X-ray band detected with *XMM-Newton* and *INTEGRAL*, respectively, can be explained as the synchrotron radiation of the electrons/positrons injected in the PWN; and (3) the VHE γ-rays in the TeV band are mainly produced via IC scattering of the electrons/positrons injected in the nebula on the CMB and interstellar IR photons.

With a sub-energetic explosion ($E_{\rm sn} \sim 0.4 \times 10^{50}$ erg), an age of $\sim$1200 yr, and an ambient density of 1.4 cm^{-3}, the radius of the composite SNR G12.8-0.0, 1.7 pc, as well as the multiband observed nonthermal fluxes for the remnant can be reproduced within the model described in this paper. The present value of the SNR shock's velocity is about 1000 km s^{-1}, and the VHE γ-rays are predominantly produced from the nebula inside the remnant via IC scattering. Of course, p–p interaction from the SNR shell can be enhanced with a denser medium around the remnant (Figure 6). Even if this condition were satisfied, the γ-rays produced via IC scattering in the PWN remain significant; hence, in this case, both the SNR shell and the PWN would contribute to the production of the observed γ-ray flux. In GeV γ-rays, the spectral property of the resulting emission in this SNR-dominated scenario (Figure 6) differs significantly from that in the PWN-dominated case (Figure 4). The VHE γ-rays of HESS J1813-178 detected with H.E.S.S. can be naturally explained as the IC scattering of the electrons/positrons injected into the PWN although the p–p collisions become important with a denser ambient medium for the remnant. Our study gives more insights into the nature of the multiband nonthermal emission of the composite SNR G12.8-0.0, even though some assumptions are made in the model.

We are very grateful to the anonymous referee for his/her helpful comments to improve the paper. This work is partially supported by the Scientific Research Foundation of Graduate School of Yunnan University, the National Natural Science Foundation of China (NSFC 10778702, 10803005), a 973 Program (2009CB824800), and Yunnan Province under grant 2009 OC.

REFERENCES

Aharonian, F., et al. (HESS Collaboration) 2005a, Science, 307, 1938
Aharonian, F., et al. (HESS Collaboration) 2005b, A&A, 437, L7
Aharonian, F., et al. (HESS Collaboration) 2006, ApJ, 636, 777
Aharonian, F., et al. (HESS Collaboration) 2007, A&A, 464, 235
Albert, J., et al. 2006, ApJ, 637, L41
Amato, E., Blasi, P., & Gabici, S. 2008, MNRAS, 385, 1946
Atoyan, A. M., & Aharonian, F. A. 1996, MNRAS, 278, 525
Berezhko, E. G., Ksenofontov, L. T., & Völk, H. J. 2002, A&A, 395, 943
Berezhko, E. G., & Völk, H. J. 2004, A&A, 419, L27
Berezhko, E. G., & Völk, H. J. 2006, A&A, 451, 981
Berezhko, E. G., & Völk, H. J. 2010, A&A, 511, 34
Blasi, P. 2002, Astropart. Phys., 16, 429
Blasi, P. 2010, MNRAS, 402, 2807
Blasi, P., Gabici, S., & Vannoni, G. 2005, MNRAS, 361, 907
Brogan, C. L. 2005, ApJ, 629, L105
Caprioli, D., Amato, E., & Blasi, P. 2010a, Astropart. Phys., 33, 160
Caprioli, D., Amato, E., & Blasi, P. 2010b, Astropart Phys., 33, 307
Caprioli, D., Blasi, P., Amato, E., & Vietri, M. 2009, MNRAS, 395, 895
Chevalier, R. A., & Liang, E. P. 1989, ApJ, 344, 332
Ellison, D. C., Berezhko, E. G., & Baring, M. G. 2000, ApJ, 540, 292
Fang, J., & Zhang, L. 2008, MNRAS, 384, 1119
Fang, J., & Zhang, L. 2010, A&A, in press (arXiv:1003.1656)
Fang, J., Zhang, L., Zhang, J. F., Tang, Y. Y., & Yu, H. 2009, MNRAS, 392, 925
Funk, S., et al. 2007, A&A, 470, 249
Gaensler, B. M., & Slane, P. O. 2006, ARA&A, 44, 17
Gelfand, J. D., Gaensler, B. M., Slane, P. O., Patnaude, D. J., Hughes, J. P., & Camilo, F. 2007, ApJ, 663, 468
Gelfand, J. D., Slane, P. O., & Zhang, W. 2009, ApJ, 703, 2051
Gotthelf, E. V., & Halpern, J. P. 2009, ApJ, 700, L158
Helfand, D. J., Gotthelf, E. V., Halpern, J. P., Camilo, F., Semler, D. R., Becker, R. H., & White, R. L. 2007, ApJ, 665, 1297
Kamae, T., Karlsson, N., Mizuno, T., Abe, T., & Koi, T. 2006, ApJ, 647, 692
Malkov, M. A., & Drury, L. O'C. 2001, Rep. Prog. Phys., 64, 429
Morlino, G., Amato, E., & Blasi, P. 2009a, MNRAS, 392, 240
Morlino, G., Amato, E., Blasi, P., & Caprioli, D. 2009b, arXiv:0912.2972
Renaud, M., et al. 2010, ApJ, 716, 663
Slane, P. 2008, in AIP Conf. Proc. 1085, High Energy Gamma-Ray Astronomy, ed. F. A. Aharonian, W. Hofmann, & F. Rieger (Melville, NY: AIP), 120
Slane, P., Castro, D., Funk, S., Uchiyama, Y., Lemiere, A., Gelfand, J. D., & Lemoine-Goumard, M. 2010, arXiv:1004.2936
Slane, P., Helfand, D. J., Reynolds, S. P., Gaensler, B. M., Lemiere, A., & Wang, Z. 2008, ApJ, 676, L33
Spitkovsky, A. 2008, ApJ, 682, L5
Truelove, J. K., & McKee, C. F. 1999, ApJS, 120, 299
Ubertini, P., et al. 2005, ApJ, 629, L109
Venter, C., & de Jager, O. C. 2006, in Proc. 363rd WE-Heraeus Seminar, Neutron Stars and Pulsars, ed. W. Becker & H. H. Huang (MPE Report 291; Garching: MPE), 40
Volpi, D., Del Zanna, L., Amato, E., & Bucciantini, N. 2008, A&A, 485, 337
Zhang, L., Chen, S. B., & Fang, J. 2008, ApJ, 676, 1216
Zirakashvili, V. N., & Aharonian, F. 2007, A&A, 465, 695